Desalination and Water Treatment
www.deswater.com
doi: 10.5004/dwt.2019.23482

147 (2019) 173–182
April

Removal of some heavy metal ions from water using novel adsorbent based on iron oxide-doped sol-gel organic-inorganic hybrid nanocomposite: equilibrium and kinetic studies

Mehdi Esmaeili Bidhendi[a,*], Mohammad Ali Gabris[b], Venus Goudarzi[c], Sara Abedynia[c], Binta Hadi Juma[d], Hassan Sereshti[b,*], Muhammad Afzal Kamboh[e], Mustafa Soylak[f,*], Hamid Rashidi Nodeh[b,g]

[a]*School of Environment, College of Engineering, University of Tehran, P.O. Box 14155-6135, Tehran, Iran, email: albintu2@gmail.com*
[b]*Department of Chemistry, Faculty of Science, University of Tehran, Tehran, Iran, emails: sereshti@ut.ac.ir (H. Sereshti), mohammadaligabris@gmail.com (M.A. Gabris), rnhamid2@gmail.com (H.R. Nodeh)*
[c]*Department of Environment, Kish International Campus, University of Tehran, Kish Island, Iran, emails: Venus.goodarzi@ut.ac.ir (V. Goudarzi), Sara.abedynia@ut.ac.ir (S. Abedynia)*
[d]*Department of Chemistry, College of Science, University of Hafar Al Batin, P.O. Box 1803, Hafar Al Batin 31991, Saudi Arabia, email: albintu2@gmail.com*
[e]*Department of Chemistry, Shaheed Benazir Bhutto University, Shaheed Benazirabad, Sindh, Pakistan, email: afzal82_kamboh@yahoo.com*
[f]*Department of Chemistry, Faculty of Sciences, Erciyes University, 38039 Kayseri, Turkey, email: soylak@erciyes.edu.tr*
[g]*Department of Food Science & Technology, Faculty of Food Industry and Agriculture, Standard Research Institute (SRI), Karaj P.O. Box 31745-139, Iran*

Received 11 May 2018; Accepted 18 November 2018

ABSTRACT

A new magnetic inorganic-organic hybrid adsorbent (*M-N*-[3-(trimethoxysilyl)propyl]ethylenediamine (TSD)-(3-glycidoxypropyltrimethoxysilane (GPTS)) was successfully synthesized via sol-gel method upon the combination of iron oxide nanoparticles and inorganic silica framework precursors (GPTS and TSD). The newly synthesized *M*-TSD-GPTS adsorbent was applied for the removal of several heavy metal ions from aqueous media. It was then characterized for its structure and composition by Fourier transform infrared, energy-dispersive X-ray spectroscopy, and scanning electron microscopy analyses. The mechanism of the adsorption process onto the magnetic organic grafted silica network may be mainly described by electrostatic interactions between the negatively charged functionalities over the adsorbent and the positively charged metal ions. Therefore, it was seen that metal ion removal was strongly dependent on the pH and adsorbent dosage, which were studied to express their influences on the overall efficiency. Adsorption kinetics and isotherms were conducted, and the adsorption mechanism was tested by two simple kinetic models pseudo-first and second order, and the kinetic parameters of the models were calculated and discussed. Langmuir and Freundlich isotherms were applied as well for this purpose. Appropriate adsorption capacities were obtained for Cd^{2+} (50.25 mg/g), Co^{2+} (30.86 mg/g), Cr^{3+} (23.25 mg/g), Ni^{2+} (28.90 mg/g), Pb^{2+} (69.44 mg/g), and V^{3+} (30.39 mg/g). Finally, the evaluation of the adsorption capability of the newly devised magnetic adsorbent showed that this material is a good candidate for all the examined metal ions.

Keywords: Magnetic iron oxide nanoparticles; 3-Glycidoxypropyltrimethoxysilane; *N*-[3-(trimethoxysilyl) propyl]ethylenediamine; Inorganic-organic hybrid sorbent; Equilibrium and kinetic studies

* Corresponding authors.

1. Introduction

Water pollution is rising globally with life-threatening diseases due to the uncontrollable population growth and the rapid expansion of industrial and agricultural activities [1]. Heavy metal ion-associated pollution has become the most serious global environmental issue [2]. Heavy metals are elements with atomic weights in the range of 63.546 and 200.590 and specific gravities greater than 4.0 [3]. Elements including Co^{2+}, Cr^{3+}, Cu^{2+}, Fe^{3+}, Mn^{2+}, Mo^{2+}, V^{3+}, Sr^{2+}, and Zn^{2+} are known as essential metals but needed only in trace levels as their excessive amounts may be deleterious to organisms [4,5]. However, elements such as Hg^{2+}, Pb^{2+}, Cd^{2+}, etc. are nonessential metals and considered as the greater threat to humans, plants, animals, as well as aquatic life. The most common source of metal ions' overload in natural water bodies traces back to various industries and other human activities [6]. Several methods have been developed for heavy metal removal from water including sedimentation, reverse osmosis, ion exchange, electroplating, biological methods, diffusive gradient technique, and adsorption via different solid materials such as activated carbon [7–9]. Whilst the previously mentioned methods are of low efficiencies and provide nonsatisfactory results in trace level removal, adsorption appears as a highly efficient attractive removal method for a variety of substances including heavy metals [10,11]. Over the recent years, nanomaterials have been widely used in removing heavy metals due to the unique advantages such as nontoxic nature, much higher adsorption capacities, and selectivity compared with traditional sorbents [12–14]. Activated carbon often suffers from extreme disadvantages such as high production and maintenance expenses, high energy and chemical requirements, low efficiency, high sludge production, sludge disposal problems, and the costly non-straightforward process of regeneration [15,16]. In the present study, functionalized nanosized nanoparticles were developed to improve the functional quality of nano-compounds enhancing interaction and decontamination efficiency as well as safety, anti-agglomeration, and cost effectiveness of the material [17–19]. Fe_3O_4 nanoparticles seem to possess very promising functionalities due to their large surface-to-volume ratio, easy incorporation and synthesis, convenient recycling, and absence of secondary contamination emissions [20,21]. Above all, the incorporation of magnetic nanoparticles (MNPs) into the adsorbent material offers the benefit of quick simple isolation of the system saving time, cost, and effort [22]. Meanwhile, organically modified silicates are inorganic-organic hybrids that combine the chemical and mechanical properties of both organic and inorganic comprising components [23,24]. The Mixture of materials shows superior properties to individual components, for example, the organic/inorganic combination produces porous structures that can be easily modified to further improve their properties. Recently, sol-gel method has been considered one of the best organic-inorganic hybrid synthesis routes because of the mild simple reaction conditions such as low room temperature and there is no need for extreme pH or free initiator radicals [25–27]. It is a suitable method to provide cheap efficient adsorbents starting from alkoxides and displaying large reactivity and surface area as well as the organic grafted –Si surface functional groups which play a big role in the capture of pollutants particularly metal ions [28–30]. Mesoporous silica-based nanomaterials are characterized by large surface areas, thus leading to their extensive application especially in adsorption, catalysis, and chromatography, as well as the defined pore sizes and shapes and the improved surface properties added by the anchored functionalities [31]. Previous studies have reported successful synthesis and application of different silica-based sol-gel hybrid materials [32–34]. Additionally, sol-gel-derived organic-inorganic hybrid materials have also been successfully used for metal ion remediation from environmental water [25,26,35,36]. These hybrid materials showed facile silica-based framework formation from the siloxane and organosiloxane precursors. Furthermore, the sandwich-like framework structure embedding an organic functional core was modified with tetraethylorthosilicate (TEOS) and *N*-[3-(trimethoxysilyl)propyl]ethylenediamine (TSD) using Stöber method [37,38]. The TSD-TEOS framework forms a massive hollow site and an oxygen linkage to increase the selectivity toward metal ions. Furthermore, *M*-TSD-3-glycidoxypropyltrimethoxysilane (GPTS) possesses two different types of amine groups (NH_2 and CNH) that can retain metal ions through the complex formation, hydrogen bonding, and electrostatic attraction which was previously confirmed by Chandra et al. (2009) who reported the possible interaction between Ni(II) ions and amine groups [39].

In this study, a hybrid network based on silica compound (TSD and GPTS) was assembled together for the first time and simultaneously magnetized. The removal efficiency of the newly synthesized magnetic silica-based inorganic-organic monohybrid was reported on several metal ions. The effects of the critical parameters on adsorption were investigated and optimized in order to obtain the maximum possible efficiency. The adsorption kinetics and mechanism were demonstrated by carrying out batch removal experiments. All the parameters relevant to the applied models were determined and discussed.

2. Experimental

2.1. Chemicals and reagents

GPTS, TSD, $FeCl_2{\cdot}4H_2O$ (2 g), $FeCl_3{\cdot}6H_2O$, $CdCl_2$, $CoCl_2$, $CrCl_3$, $NiCl_2$, $Pb(NO_3)_2$, V_2O_3, ammonium hydroxide, and ethanol were obtained from Merck Company (Darmstadt, Germany).

2.2. Instruments

A field emission scanning electron microscope from MIRA3 TESCAN (Prague, Czech Republic) operated at 10 kV was used to examine the surface morphology of the synthesized nano hybrid. Fourier transform infrared (FTIR) spectrum was recorded using an Equinox 55 FTIR spectrometer (Bruker, Bremen, Germany) scanning the wave number range of 450–4,000 cm^{-1} in spectral-grade KBr pellets. All absorbance measurements were obtained by a Perkin Elmer AAnalyst 400 atomic absorption spectrometer (Uerlingen, Germany) equipped with an electrodeless discharge lamp for the given ions. Crystallinity of the nanocomposite was studied with X-ray diffractometer (XRD) from Bruker (Germany) with

condition of Cu Kα cathode (λ = 1.54060 Å), voltage 40 kV, and current 40 mA. Zeta potential of the nanocomposite at different pH was investigated with Z100 HORIBA Scientific analyzer (Tokyo, Japan). Brunauer-Emmett-Teller (BET) specific surface area and pore size of the nanocomposite were obtained with BET N_2 adsorption-desorption method using Belsorp-mini II instrument, BEL Japan Inc. (Osaka, Japan).

2.3. Synthesis of M-TSD-GPTS

First, MNPs (*M*) were synthesized using $FeCl_2{\cdot}4H_2O$ (2 g) and $FeCl_3{\cdot}6H_2O$ (1 g) by dissolving in 30 mL of distilled water. The solution was heated until 50°C, and then 1.5 mL ammonium hydroxide solution was added dropwise into the solution followed by stirring for 5 h. The obtained product (*M*) was washed with the excess of deionized water and oven dried at 80°C for 24 h.

The prepared MNPs were joined to the silica-based hybrid organic-inorganic framework to produce *M*-TSD-GPTS (Fig. 1). Briefly, the MNPs (0.5 g) were dispersed in the mixture solution of 40 mL ethanol and 1 mL aqueous solution of NH_3 (25%). Then, 1 mL of TSD in 4 mL ethanol was added into the reaction mixture to form the first layer of organic silica framework [38]. Thereafter, 2 mL GPTS in 9 mL ethanol was added to form the outer layer to form sol-gel hybrid TSD-GPTS on the surface of MNPs (*M*-TSD-GPTS). The mixture was kept at 30°C for 3 h, isolated with the help of external magnet, washed with ethanol and excess water, and oven dried at 80°C for 24 h.

2.4. Procedure

Batchwise removal experiments of several metals, namely, Cd^{2+}, Co^{2+}, Cr^{3+}, Ni^{2+}, Pb^{2+}, and V^{3+} onto the proposed adsorbent were carried out in 40 mL solution volume and 50 mg/L of initial concentration. The different effective parameters were investigated such as solution pH (2.0–7.0), the mass of adsorbent (5–120 mg), and contact time (10–230 min). With each adsorption experiment, the adsorbent suspension containing the adsorbate was withdrawn after a certain time using an external magnet and the residual metal concentration was measured using flame atomic absorption spectroscopy. The equilibrium adsorption capacity q_e (mg/g) and removal efficiency (*R*%) were calculated according to Eqs. (1) and (2), respectively.

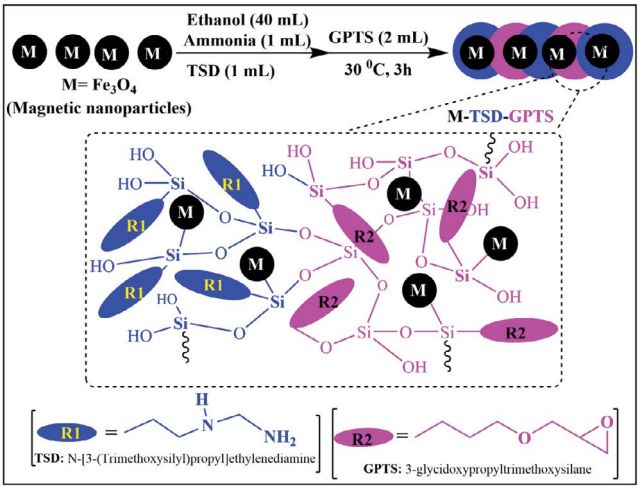

Fig. 1. Graphical scheme illustrating the synthesis procedure of silica-based hybrid organic-inorganic framework (*M*-TSD-GPTS).

$$q_e = \frac{V\left(C_0 - C_e\right)}{m} \tag{1}$$

$$R\% = \frac{\left(C_0 - C_e\right)}{C_0} \times 100 \tag{2}$$

where *m* is the adsorbent dosage in gram (g), C_0 and C_e are the concentrations of the different metals before and after adsorption in mg/L, and *V* is the volume of the aqueous phase in 1 L.

The adsorption isotherm study was carried out at a given temperature and time after setting all the effective experimental parameters at their corresponding optimum values.

3. Results and discussion

3.1. Characterization

Scanning electron microscopy (SEM), the morphology and surface properties of the prepared material were investigated using SEM. Fig. 2(a) shows the porous nature of the material with large voids and cavities. The colloid suspension structure of the silica framework can be seen too. This indicates that the silica framework was successfully achieved. Besides, the MNP aggregations sprinkled throughout the inorganic-organic hybrid substrate can be clearly observed.

Energy-dispersive X-ray spectroscopy (EDX), The elemental analysis of the designed adsorbent was performed using EDX. The successful synthesis was confirmed by the elemental composition of the silica-based inorganic-organic nano hybrid. According to the spectrum present in Fig. 2(b), all the expected elements (Si, C, O, and N) were observed clearly. Besides, the extra element (Fe) corresponding to the magnetic Fe_3O_4 nanoparticles was also present, thereby confirming the successful formation of the desired nano hybrid.

BET, in further experiments, the sorption capacity of the nanocomposite was investigated based on nitrogen adsorption-desorption principal through BET technique, thus specific surface area obtained was 69 g^2 m^2 and Barrett-Joyner-Halenda pore volume obtained was 0.059 cm^3/g. This technique predicted mesoporous structure for *M*-TSD-GPTS due to its pore diameter (4.91 nm).

FTIR, the infrared spectrum given in Fig. 3 indicated the success of the synthesis process particularly through the absence of 1,260 cm^{-1} peak as an evidence for epoxy ring opening and reaction occurrence. The presence of the silica matrix could be verified by the following peaks: 467 cm^{-1}, 787 cm^{-1}, 1,055 cm^{-1}, and 3,337 cm^{-1} assigned to siloxane (Si–O–Si) and adsorbed water (H–O–H) bending vibrations and silica (Si–O), siloxane (Si–O–Si), and silanol (Si–OH) stretching vibrations, respectively [40–42]. Furthermore, the slightly broad peak occurring at 3,300 cm^{-1} can be traced back to the amine groups existing in the material which fulfills the aim of this project of having an enhanced adsorption

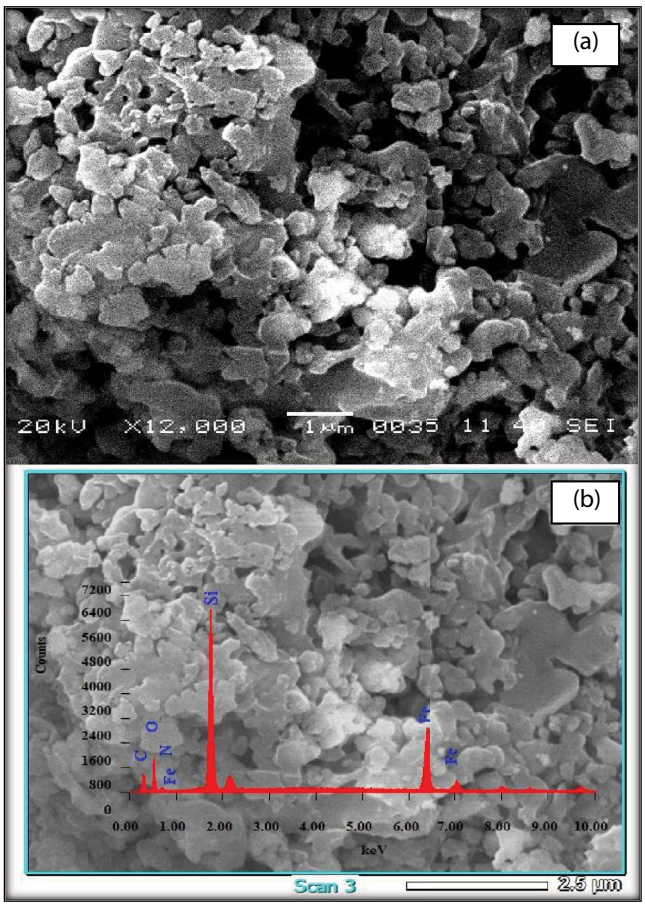

Fig. 2. Figure represents the (a) SEM micrograph of the as-prepared hybrid nanocomposite and (b) EDX spectrum and elemental composition of the *M*-TSD-GPTS nanocomposite.

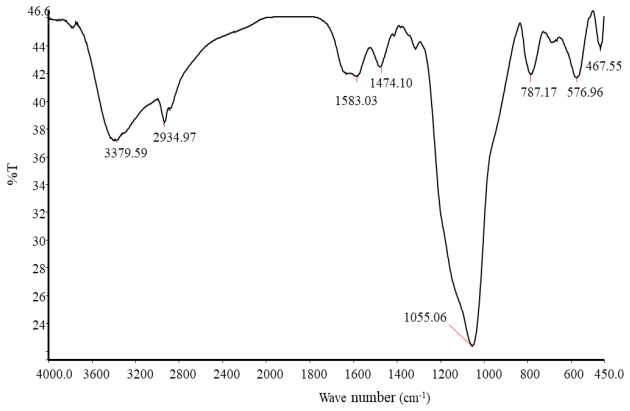

Fig. 3. FTIR spectrum of the newly prepared hybrid nanocomposite.

capacity of the reported material. The peaks at 1,583 cm^{-1} and 1,312 cm^{-1} are corresponding to C–N and N–H groups in TSD structure, respectively [43]. Finally, the organic insertion was confirmed by the peak at 2,934 cm^{-1} attributed to C–H stretching by the time the added magnetic property [44,45] was depicted by the characteristic peak located at 576 cm^{-1} (Fe–O) [46].

XRD, crystallinity of the magnetic *M*-TSD-GPTS nanocomposite was studied with XRD. Fig. 4 shows the XRD pattern for the plain MNPs and magnetic adsorbent (*M*-TSD-GPTS). XRD signals for MNPs (labeled as 1) were observed at 2 theta of 30.5°, 35.2°, 43.1°, 53.5°, 57.9°, and 62.1°. These are indicating crystalline structure for MNPs. XRD pattern for *M*-TSD-GPTS nanocomposite shows three extra signals when compared with MNPs. The broad characteristic peak at 2 theta of 22.5° (label 2) is corresponding to amorphous silica network. The two sharp signals at 2 theta of 17.2° and 28.1° (label 3) are probably related to TSD-GPTS network. Hence, based on these two signals, it can be claimed that the TSD-GPTS network is in crystalline properties.

3.2. pH study

Since adsorption process may be explained by electrostatic interaction between the negatively/positively charged adsorbent functionalities and metal cations, solution pH will play an imperative role. Adsorbent surface charge was investigated via zeta potential analysis and its values obtained in the range of +20 to –15.6 at pH 2–10. Thus, pH of point zero charge (pH_{PZC}) obtained at pH 4.8 means *M*-TSD-GPTS has positive charge at pH 4.8 and negative charge at pH > 4.8. The impact of solution pH on removal efficiency of metal ions (Cd^{2+}, Co^{2+}, Cr^{3+}, Ni^{2+}, Pb^{2+}, and V^{3+}) using designed nano hybrid material was studied in the pH range of 2–7. The results obtained were represented in Fig. 5(a). As expected, the removal efficiency of metals increased with increasing pH because at low pHs, the functional groups present on the surface of the adsorbent (silanol and amine groups) are more protonated and thus less favorable to retain the positive occurring metallic species that are generally present as cations at pH < 5. The low adsorption at low pH may be attributed to the competition of H^+ to the adsorption sites on the adsorbent present. The other reason for such behavior is the different structures of their aqua anions with pH that either support or weaken the adsorption. At different pHs, metal ions exist in different states as follows: cadmium [Cd(II)]: pH 2–8.5 (Cd^{2+}), 8.6–10.5 ($Cd(OH)^-$), 10.6–12 $(Cd(OH)_2)_{aq}$ [47]; cobalt [Co(II)]: pH 1–8.5 (Co^{2+}), 8.6–9.5 ($Co(OH)^-$), 9.6–12 $(Co(OH)_2)$ [48]; chromium [Cr(III)]: pH 1–3 (Cr^{3+}), 3.1–6 ($Cr(OH^{2+})$), 6.1–8 $(Cr(OH^+)_2)$, 8–2 $(Cr(OH)_3)$ [49]; nickel [Ni(II)]: pH 2–6.1 (Ni^{2+}), 6.2–12 $(Ni(OH)_2)$ [50]; lead [Pb(II)]: pH 1–6.1 (Pb^{2+}), 6.2–8.5 (Pb(OH)), 8.6–11 $(Pb(OH)_2aq)$ [51]; and vanadium [V(III)]: pH 2–3 (VO_2^+), 3.1–4 $(VO(OH)_3)$, 4.1–8.5 $(VO_2(OH)_2^-)$, 8.6–10 $(VO_3(OH)^{2-})$. Therefore, the slight increase in pH positively affects the overall efficiency of adsorption via better attraction and enhances the performance of the designed adsorbent (Fig. 5(b)). This might be due to the adsorbent surface functional groups (N–H and Si–O) experiencing suitable protonation/deprotonation transition at this stage and thus providing more metal removal [52]. Highly basic media are not recommended because of the negative charge of the adsorbate associated with the competition of OH^- ions and deprotonation of the adsorbent surface functional groups causing repulsion instead of adsorption [53]. According to the results obtained, the slightly basic medium was chosen for the efficient sensitive detection of the metal ions.

3.3. Adsorbent dosage study

The optimum amount of adsorbent needed for the quantitative removal of adsorbate is described by the mass of adsorbent. Referring to Fig. 5(c), it can be seen that for all the metal ions, the same increasing trend was obtained but the quantitative adsorption capability of the sorbent material was slightly different and defined in the order $V^{2+} < Cr^{3+} < Ni^{2+} \cong Co^{2+} \cong Pb^{2+} \cong Cd^{2+}$.The increase could be attributed to the availability of more adsorption sites on the solid phase with lower adsorbent amounts while the constant level was due to the decrease in surface area at large dosages and the saturation of adsorption sites. So the optimum adsorbent dosage was almost 80 mg for all metals to obtain nearly maximum removal efficiency.

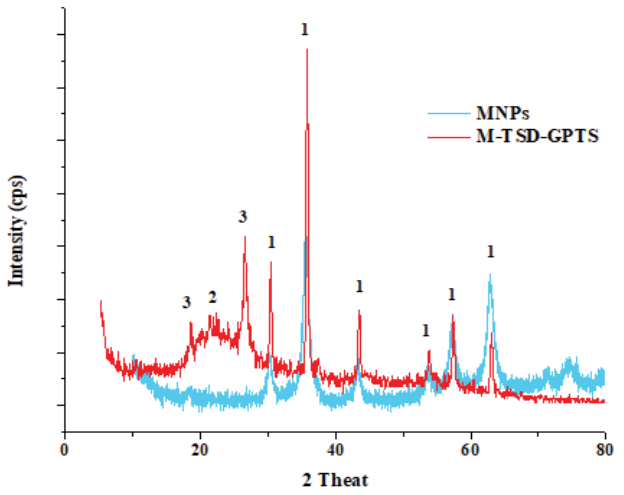

Fig. 4. XRD pattern for magnetic nanoparticles and magnetic sol-gel organic-inorganic hybrid nanocomposite.

3.4. Time study

Metal adsorption was studied kinetically via batch experiments at different contact times in the range of 10–80 min. The plots represent the amounts adsorbed q_t versus time for an initial concentration of metal ions. As can be seen, almost the same increasing time profiles were obtained for all the metal ions. Adsorption was considered very fast as equilibrium was achieved within a very short time of 80 min. The trends as shown in Fig. 6 were not very sharp implying that the kinetic difference was not too serious, and nearly in the first 10 min, the majority of the metal was adsorbed and removed. As well known, the increase in q_e with the increasing initial concentration of adsorbate confirmed the fact that the greater the time and amount available the stronger the concentration flux and the higher the maximum amount extracted at equilibrium. The equilibrium time was the same among all metals so a very similar kinetic rate was proposed to these metals. The fast metal uptake may be attributed to the large availability of silanol groups on the backbone of the adsorbent. The isotherms suggest two-stage mechanism: rapid first portion during the first 60 min and slow one after

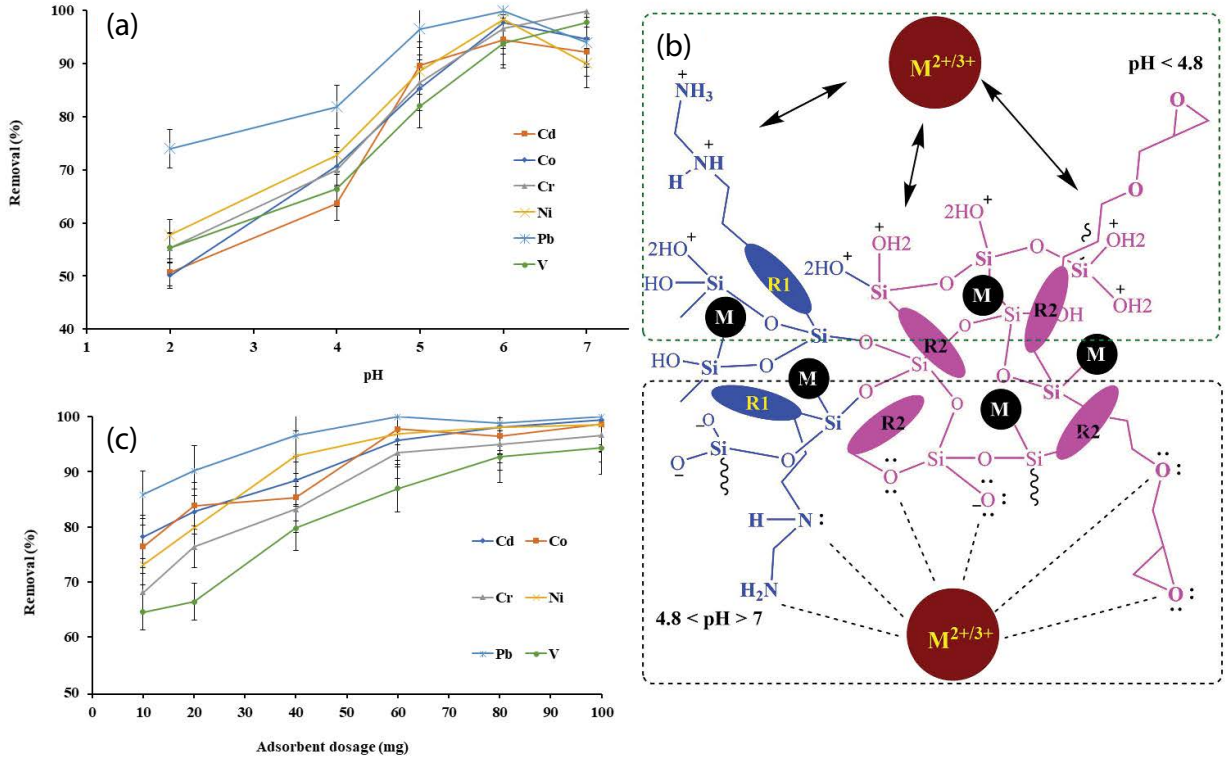

Fig. 5. (a) Effect of solution pH on metal ion removal, (b) proposed mechanism for metal ion adsorption onto *M*-TSD-GPTS at different pH based on zeta potential (pH_{ZPC} 4.8), and (c) effect of mass of adsorbent on removal efficiency.

equilibrium. This two-phase adsorption may be illustrated by the easy physical adsorption of adsorbates over the early more freely available surface followed by a slow late stage accompanied by the decrease in the availability of the adsorption sites and traffic, thus causing slowing down of the adsorption process.

3.5. Concentration study (adsorption equilibrium)

Initial concentration is another critical parameter affecting the adsorption capacity (q_e) of an adsorbent. The effect of this parameter was studied by plotting the adsorption isotherm relating the equilibrium concentration of adsorbate (q_e) on the adsorbent to that in the liquid phase (C_e) (Fig. 7). This was achieved by varying the initial concentration of the different metal ions from 10 to 100 mg/L. According to equilibrium isotherm, for all the metals, equilibrium was attained at 60 mg/L, and as the initial concentration increased, q_e increased to reach a steady state due to saturation of the adsorbent with metal ions ($M^{2+/3+}$) at the top probably due to its large size delaying the saturation of the solid sorbent. In conclusion, this result describes a single-layer adsorption system of *type I* [54].

3.6. Kinetic modeling

The adsorption rates of metal ions into the adsorbent were simply studied using two models, namely, pseudo-first and second order. First-order kinetic equation is expressed as follows [55]:

$$\ln\left(q_e - q_t\right) = \ln q_e - k_1 t \tag{3}$$

While that of second order,

$$\frac{t}{q_t} = \frac{1}{k_2 q_e^2} + \frac{t}{q_e} \tag{4}$$

where k_1 (1/min) and k_2 (g/mg min) are the adsorption rate constants of pseudo-first and second order, respectively, q_e (mg/g of dry weight) is the amount of metal ion adsorbed onto the adsorbent surface at equilibrium while q_t (mg/g) is that adsorbed at any time t (min).

According to the fact that the model possessing the better correlation coefficient (R^2) is the one describing the kinetic nature of the adsorption process; the second order was the one fitting for all the metals with values greater than 0.99, and q_e (theoretical) values closer to q_e (experimental). The different parameters including rate coefficients and the calculated equilibrium uptakes of each model were obtained from the linear models and listed in Table 1.

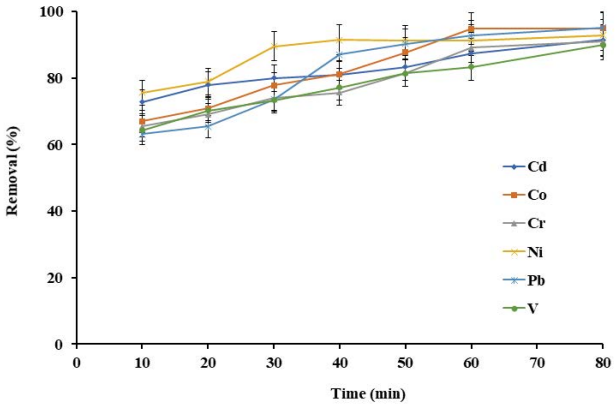

Fig. 6. Effect of contact time on removal efficiency.

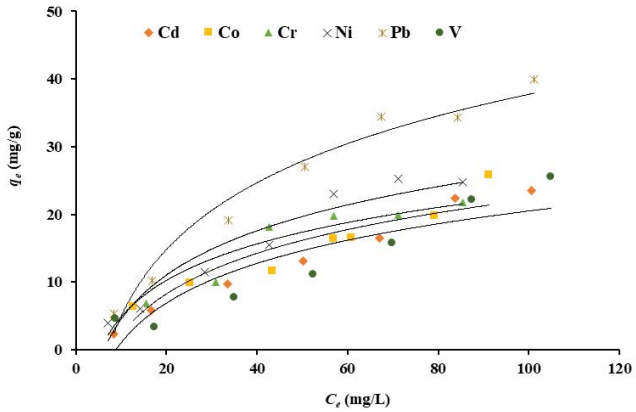

Fig. 7. Effect of initial concentration of adsorption equilibrium capacity.

3.7. Adsorption isotherm modeling

Adsorption isotherm, which is the plot of removal vs initial concentration, relates the coverage nature on the adsorbent surface to the concentration of adsorbate in solution at a given temperature to describe the adsorption equilibrium mechanism and determine the optimal amount of adsorbate needed for the quantitative extraction of the metal ion denoted by the adsorbent capacity [56]. The most common isotherm models Langmuir and Freundlich were adopted in this paper to analyze the experimental data of adsorption obtained and determine the maximum uptake of q_m (mg/g) the metals examined at different concentrations which are measured from the slope of the optimum plot. The Langmuir isotherm model is valid for monolayer adsorption onto a surface of finite identical sites. It assumes a single-layer attachment of adsorbate, conserved adsorption energy, and the absence of adsorbate transmigration. Freundlich isotherm is affiliated to both chemisorption (monolayer) and physisorption (multilayer) adsorption mechanisms.

The isotherm models can be linearly expressed according to Eqs. (5) and (6) [10,57].

$$\frac{C_e}{q_e} = \frac{C_e}{q_m} + \frac{1}{k_L q_m} \tag{5}$$

$$\ln q_e = \ln K_F + \left(\frac{1}{n}\right)\ln C_e \tag{6}$$

where q_m and q_e are the maximum and observed uptake capacities (mg/1 g of sorbent), respectively; C_e is the equilibrium concentration (mg/1 L of solution); K_L and K_F are the equilibrium constants of Langmuir and Freundlich,

Table 1
Kinetic pseudo-first-order and pseudo-second-order parameters and values for metal ions

Kinetic models	Parameters	Cd^{2+}	Co^{2+}	Cr^{3+}	Ni^{2+}	Pb^{2+}	V^{3+}
Pseudo-first order	M	0.033	0.054	0.039	0.065	0.055	0.073
	B	2.45	3.2334	2.9318	2.4868	3.35	3.78
	k_1	0.033	0.054	0.039	0.065	0.055	0.073
	q_e theory (mg/g)	11.39	24.81	18.39	11.82	27.86	42.71
	R^2	0.886	0.871	0.906	0.902	0.97	0.715
Pseudo-second order	M	0.0317	0.0261	0.0303	0.031	0.0198	0.2371
	B	0.1544	0.2514	0.2612	0.095	0.1204	0.0314
	k_2	0.0010	0.0006	0.0009	0.0009	0.0004	0.0562
	q_e (theory)	31.54	38.31	33.01	32.25	50.51	4.21
	R^2	0.995	0.992	0.988	0.999	0.9909	0.994

M: slope of linear model (Eqs. (3) and (4)); B: intercept of linear model (Eqs. (3) and (4)).

respectively; and n is the measure of the Freundlich-based adsorption intensity (if n value is between 1 and 10 implying the adsorption process is favorable).

The corresponding equations of each isotherm were plotted, and the different characteristic parameters of each model were calculated in Table 2. Based on the values of R^2, it was assumed that both Langmuir and Freundlich models apply to describe the adsorption of metal ions onto the adsorbent devised because of the high values of R^2 except for vanadium, which showed only compliance with Langmuir. The lower but acceptable values of R^2 may be attributed to the low adsorption capacities leading to higher experimental errors. As shown, the isotherm parameters obtained vary among the different metals, and the highest maximum uptake corresponds to lead. Freundlich is highly applicable to highly heterogeneous surfaces accompanied by the adsorption of several layers of adsorbate via Van der Waals forces, while Langmuir describes the monolayer coverage nature of adsorbate onto the adsorbent surface.

3.8. Coexisting

In aqueous environments, interfering ions such as phosphate, sulfate, nitrate, sodium, potassium, copper, iron, and aluminum exist because of the complicated diverse matrix with 80 mg adsorbent for 60 min shaking time. Therefore, it is important to study the effect of these coexisting ions on the adsorption process. For this purpose, solutions with concentration of target metals: 50 mg/L and interferences: Al^{3+}, Fe^{3+}, Cu^{2+}, Zn^{2+}, Na^{+}, K^{+}, Cl^{-}, Br^{-}, SO_3^{2-}, PO_4^{3-}, NO_3^{-} are in 500 mg/L were prepared and each time the same removal procedure was done repeatedly, and lastly the concentrations of the main metals were measured to notice the changes. The removal efficiency (R%) obtained were 86.6%, 73.7%, 85.5%, 79.8%, 88.1%, and 70.6% for Cd^{2+}, Co^{2+}, Cr^{3+}, Ni^{2+}, Pb^{2+}, and V^{3+}, respectively. The high removal efficiencies showed the high affinity of the metal ions toward the devised adsorbent even in the presence of interfering ions, which implied the high selectivity of the adsorbent and the low effect of these unwanted ions on the measurement process.

3.9. Comparison

Compared with other adsorbents reported for metal uptake, similar and comparable capacities can be seen in Table 3. The difference in capacities can be explained by the pH dependence and the silica porous unique structure. The easy recovery of the adsorbent-adsorbate system simply

Table 2
Langmuir and Freundlich isotherm parameters and values for metal ions

Isotherms	Parameters	Cd^{2+}	Co^{2+}	Cr^{3+}	Ni^{2+}	Pb^{2+}	V^{3+}
Langmuir	M	0.019	0.032	0.043	0.034	0.014	0.032
	B	3.084	1.238	0.273	0.463	0.1289	0.339
	q_m (mg/g)	50.25	30.86	23.25	28.90	69.44	30.39
	K_L	0.041	0.071	0.150	0.12	0.141	0.112
	R^2	0.902	0.935	0.993	0.981	0.991	0.936
Freundlich	M	0.788	0.456	0.334	0.469	0.379	0.496
	B	0.644	0.997	1.703	1.26	2.174	1.409
	K_F	1.89	2.69	5.42	3.49	8.66	4.05
	N	1.26	2.19	2.99	2.13	2.638	2.01
	R^2	0.992	0.985	0.905	0.951	0.958	0.794

M: slope of linear model (Eqs. (5) and (6)); B: intercept of linear model (Eqs. (5) and (6)).

Table 3
Comparison of current study with previously published works in terms of time, pH, and sorption capacity

Adsorbent	Metal ions	pH	Ads. Time (min)	q_e (mg/g)	Ref.
Cortex fruit wastes	Cd^{2+}, Zn^{2+}, Cr^{3+}	6	60	195–470	[58]
Waste treatment sludge	V^{3+}	4	–	37.17	[59]
MCM-41, MCM-48	Cd^{2+}, Co^{2+}, Cu^{2+}, Pb^{2+}	5.5	60	27.66	[60]
Sol-gel organic–inorganic hybrid	Sb^{2+}	5	20	108	[41]
Sol-gel organic-inorganic hybrid	Cd^{2+}, Pb^{2+}, Cu^{2+}	5–6	30	13.3–56.7	[36]
Sol-gel organic-inorganic hybrid	Pb^{2+}	5.5	30	54.9	[35]
Hybrid silica	Pb^{2+}, Cd^{2+}	–	60	102.02, 94.05	[61]
Magnetic sol-gel organic-inorganic hybrid	Cd^{2+}, Co^{2+}, Cr^{3+}, Ni^{2+}, Pb^{2+}, and V^{3+}	6	60	23–69	Present work

using a magnet without additional expense effort and time-consuming steps is the most interesting advantage of the new adsorbent. Finally, the fast removal of metals can be clearly mentioned.

4. Conclusion

In this study, new magnetic nanocomposite based on sol-gel organic-inorganic hybrid material (*M*-TSD-GPTS) was synthesized and applied for several toxic metal ion removal from aqueous solution. The organic functionalities introduced into the inorganic framework of silica have improved the adsorption capability of the material as a whole. The added magnetism facilitated its collection and separation from the sample matrix. Out of the applied kinetic models, pseudo-second order turned out to be more properly describing the contact time data. Both adsorption isotherm models (Langmuir and Freundlich) fitted with the experimental data for all the metals examined. The maximum adsorption capacity (q_m) from Langmuir isotherm was obtained for all metal ion uptake onto material *M*-TSD-GPTS found to be in the range of 23–69 mg/g at pH 6. The proposed nanocomposite provided high affinity toward two valent metal ions as compared with three valent ions ($Pb^{2+} > Cd^{2+} > Co^{2+} > V^{3+} > Cr^{3+}$). Hence, the newly introduced organic-inorganic hybrid nanocomposite can be used as solid adsorbent in water treatment process.

Acknowledgment

Authors would like to thank University of Tehran and Parseen (Pars Environment, Energy and Nanotechnology) Corporation for the facilities and financial support.

References

[1] P.N. Dave, L.V. Chopda, Application of iron oxide nanomaterials for the removal of heavy metals, J. Nanotechnol., 2014 (2014) 14 p.
[2] R. Abu-El-Halawa, S.A. Zabin, Removal efficiency of Pb, Cd, Cu and Zn from polluted water using dithiocarbamate ligands, J. Taibah Univ. Sci., 11 (2017) 57–65.
[3] T. Shibamoto, L. Bjeldanes, Introduction to Food Toxicology, 2nd Ed., Elsevier, Burlington, 2009.
[4] N. Neyaz, W.A. Siddiqui, K.K. Nair, Application of surface functionalized iron oxide nanomaterials as a nanosorbents in extraction of toxic heavy metals from ground water: a review, Int. J. Environ. Sci., 4 (2013) 472–483.
[5] R. Aravindhan, B. Madhan, J.R. Rao, B.U. Nair, T. Ramasami, Bioaccumulation of chromium from tannery wastewater: an approach for chrome recovery and reuse, Environ. Sci. Technol., 38 (2004) 300–306.
[6] U.N. Bhat, A.B. Khan, Heavy metals: an ambiguous category of inorganic contaminants, nutrients and toxins, Res. J. Environ. Sci., 5 (2011) 682–690.
[7] J. Fan, M. Qi, R. Fu, L. Qu, Performance of graphene sheets as stationary phase for capillary gas chromatographic separations, J. Chromatogr. A, 1399 (2015) 74–79.
[8] F. Ciesielczyk, P. Bartczak, T. Jesionowski, Removal of nickel (II) and cadmium (II) ions from aqueous solutions using an oxide adsorbent of MgO SiO_2 type, Desal. Wat. Treat., 55 (2015) 1271–1284.
[9] F. Ciesielczyk, P. Bartczak, J. Zdarta, T. Jesionowski, Active MgO–SiO_2 hybrid material for organic dye removal: a mechanism and interaction study of the adsorption of CI Acid Blue 29 and CI Basic Blue 9, J. Environ. Manage., 204 (2017) 123–135.
[10] H.R. Nodeh, H. Sereshti, E.Z. Afsharian, N. Nouri, Enhanced removal of phosphate and nitrate ions from aqueous media using nanosized lanthanum hydrous doped on magnetic graphene nanocomposite, J. Environ. Manage., 197 (2017) 265–274.
[11] W.A.W. Ibrahim, H.R. Nodeh, M.M. Sanagi, Graphene-based materials as solid phase extraction sorbent for trace metal ions, organic compounds, and biological sample preparation, Crit. Rev. Anal. Chem., 46 (2016) 267–283.
[12] X. Wang, Y. Guo, L. Yang, M. Han, J. Zhao, X. Cheng, Nanomaterials as sorbents to remove heavy metal ions in wastewater treatment, J. Environ. Anal. Toxicol., 2 (2012) 1–5.
[13] A. Muzammil, R. Miandad, M. Waqas, F. Gehany, M.A. Barakatab, Remediation of wastewater using various nano-materials, Arabian J. Chem., (2016) , doi: https://doi.org/10.1016/j.arabjc.2016.10.004 (in Press).
[14] F. Ciesielczyk, J. Goscianska, J. Zdarta, T. Jesionowski, The development of zirconia/silica hybrids for the adsorption and controlled release of active pharmaceutical ingredients, Colloids Surf. A Physicochem. Eng. Asp., 545 (2018) 39–50.
[15] P.V. Rajasulochana P, Comparison on efficiency of various techniques in treatment of waste and sewage water – A comprehensive review, Resour.-Effic. Technol., 2 (2016) 175–184.
[16] H. Sadegh, G.A.M. Ali, V.K. Gupta, A.S.H. Makhlouf, R. Shahryari-Ghoshekandi, M.N. Nadagouda, M. Sillanpää, E. Megiel, , The role of nanomaterials as effective adsorbents and their applications in wastewater treatment, J. Nanostruct. Chem., 7 (2017) 1–14.
[17] J. Cha, S. Jin, J.H. Shim, C.S. Park, H.J. Ryu, S.H. Hong, Functionalization of carbon nanotubes for fabrication of CNT/epoxy nanocomposites, Mater. Des., 95 (2016) 1–8.
[18] R. Thiruppathi, S. Mishra, M. Ganapathy, P. Padmanabhan, B. Gulyás, Nanoparticle functionalization and its potentials for molecular imaging., Adv. Sci., 4 (2017) 1–14.
[19] F. Ciesielczyk, P. Bartczak, Ł. Klapiszewski, T. Jesionowski, Treatment of model and galvanic waste solutions of copper

(II) ions using a lignin/inorganic oxide hybrid as an effective sorbent, J. Hazard. Mater., 328 (2017) 150–159.
[20] W. Wu, Q. He, C. Jiang, Magnetic iron oxide nanoparticles: synthesis and surface functionalization strategies, Nanoscale Res. Lett., 3 (2008) 397–415.
[21] J. Xu, J. Sun, Y. Wang, J. Sheng, F. Wang, M. Sun, Application of iron magnetic nanoparticles in protein immobilization, Molecules, 19 (2014) 11465–11486.
[22] M.K.M. Nodeh, M.A. Gabris, H.R. Nodeh, M.E. Bidhendi, Efficient removal of arsenic(III) from aqueous media using magnetic polyaniline-doped strontium–titanium nanocomposite, Environ. Sci. Pollut. Res., 25 (2018) 16864–16874.
[23] S. Katayama, S. Katayama, Synthesis of Mechanically Flexible Organic–Inorganic Hybrid Nanocomposites from Polydimethylsiloxane and Metal Alkoxides, in: Hybrid Nanocomposites for Nanotechnology, Springer, Boston, MA, 2009, pp. 173–192.
[24] F. Ciesielczyk, P. Bartczak, T. Jesionowski, A comprehensive study of Cd (II) ions removal utilizing high-surface-area binary Mg–Si hybrid oxide adsorbent, Int. J. Environ. Sci. Technol., 12 (2015) 3613–3626.
[25] H.-T. Fan, Q. Tang, Y. Sun, Z.-G. Zhang, W.-X. Li, Selective removal of antimony (III) from aqueous solution using antimony (III)-imprinted organic–inorganic hybrid sorbents by combination of surface imprinting technique with sol–gel process, Chem. Eng. J., 258 (2014) 146–156.
[26] C.A. Quirarte-Escalante, V. Soto, W. de la Cruz, G.R. Porras, R. Manríquez, S. Gomez-Salazar, Synthesis of hybrid adsorbents combining sol− gel processing and molecular imprinting applied to lead removal from aqueous streams, Chem. Mater., 21 (2009) 1439–1450.
[27] F. Ciesielczyk, W. Szczekocka, K. Siwińska-Stefańska, A. Piasecki, D. Paukszta, T. Jesionowski, Evaluation of the photocatalytic ability of a sol-gel-derived MgO-ZrO_2 oxide material, Open Chem., 15 (2017) 7–18.
[28] S. Pandey, S.B. Mishra, Sol–gel derived organic–inorganic hybrid materials: synthesis, characterizations and applications, J. Sol-Gel Sci. Technol., 59 (2011) 73–94.
[29] S. Gross, K. Müller, Sol–gel derived silica-based organic–inorganic hybrid materials as "composite precursors" for the synthesis of highly homogeneous nanostructured mixed oxides: an overview, J. Sol-Gel Sci. Technol., 60 (2011) 283–298.
[30] Synthesis of hybrid materials functionalized with cyano-ionic liquid for the extraction of chlorophenols and polycyclic aromatic hydrocarbons/Shabnam Bakhshaei, Ph.D. Thesis, University of Malaya, 2016.
[31] Z. ALOthman, A review: fundamental aspects of silicate mesoporous materials, Materials, 5 (2012) 2874–2902.
[32] W.W. Ibrahim, A.A. Keyon, N. Prastomo, A. Matsuda, Synthesis and characterization of polydimethylsiloxane-cyanopropyltriethoxysilane-derived hybrid coating for stir bar sorptive extraction, J. Sol-Gel Sci. Technol., 59 (2011) 128–134.
[33] N. Muhamad, W.A.W. Ibrahim, M.M. Snagi, Sol-gel hybrid cyanopropyltriethoxysilane-methyltrimethoxysilane as adsorbent for dispersive-micro solid phase extraction of selected organophosphorus pesticides in water samples, J. Teknol., 5 (2015) 57–62.
[34] W.A.W. Ibrahim, K.V. Veloo, M.M. Sanagi, Novel sol-gel hybrid methyltrimethoxysilane-tetraethoxysilane as solid phase extraction sorbent for organophosphorus pesticides, J. Chromatogr. A, 1229 (2012) 55–62.
[35] H.-T. Fan, X.-T. Sun, W.-X. Li, Sol–gel derived ion-imprinted silica-supported organic–inorganic hybrid sorbent for selective removal of lead (II) from aqueous solution, J. Sol-Gel Sci. Technol., 72 (2014) 144–155.
[36] H.-T. Fan, Z.-J. Su, X.-L. Fan, M.-M. Guo, J. Wang, S. Gao, S. Ting, Sol–gel derived organic–inorganic hybrid sorbent for removal of Pb^{2+}, Cd^{2+} and Cu^{2+} from aqueous solution, J. Sol-Gel Sci. Technol., 64 (2012) 418–426.
[37] X. Fang, X. Zhao, W. Fang, C. Chen, N. Zheng, Self-templating synthesis of hollow mesoporous silica and their applications in catalysis and drug delivery, Nanoscale, 5 (2013) 2205–2218.
[38] D. Chen, L. Li, F. Tang, S. Qi, Facile and scalable synthesis of tailored silica "nanorattle" structures, Adv. Mater., 21 (2009) 3804–3807.
[39] S. Chandra, D. Jain, A.K. Sharma, P. Sharma, Coordination modes of a Schiff base pentadentate derivative of 4-aminoantipyrine with cobalt (II), nickel (II) and copper (II) metal ions: synthesis, spectroscopic and antimicrobial studies, Molecules, 14 (2009) 174–190.
[40] S.R. Darmakkolla, H. Tran, A. Gupta, S.B. Rananavare, A method to derivatize surface silanol groups to Si-alkyl groups in carbon-doped silicon oxides, RSC Adv., 6 (2016) 93219–93230.
[41] H.-T. Fan, W. Sun, B. Jiang, Q.-J. Wang, D.-W. Li, C.-C. Huang, W. Kang-Jun, Z. Zhi-Gang, L. Wen-Xiu, Adsorption of antimony (III) from aqueous solution by mercapto-functionalized silica-supported organic–inorganic hybrid sorbent: Mechanism insights, Chem. Eng. J., 286 (2016) 128–138.
[42] H.-T. Fan, Y. Sun, Q. Tang, W.-L. Li, T. Sun, Selective adsorption of antimony (III) from aqueous solution by ion-imprinted organic–inorganic hybrid sorbent: kinetics, isotherms and thermodynamics, J. Taiwan Inst. Chem. Eng., 45 (2014) 2640–2648.
[43] H.R. Nodeh, H. Sereshti, H. Gaikani, M.A. Kamboh, Z. Afsharsaveh, Magnetic graphene coated inorganic-organic hybrid nanocomposite for enhanced preconcentration of selected pesticides in tomato and grape, J. Chromatogr. A, 1509 (2017) 26–34.
[44] H.-T. Fan, A.-J. Liu, B. Jiang, Q.-J. Wang, T. Li, C.-C. Huang, Sampling of dissolved inorganic Sb III by mercapto-functionalized silica-based diffusive gradients in thin-film technique, RSC Adv., 6 (2016) 2624–2631.
[45] D.-P. Sui, H.-X. Chen, L. Liu, M.-X. Liu, C.-C. Huang, H.-T. Fan, Ion-imprinted silica adsorbent modified diffusive gradients in thin films technique: tool for speciation analysis of free lead species, Talanta, 148 (2016) 285–291.
[46] M.A. Gabris, B.H. Jume, M. Rezaali, S. Shahabuddin, H.R. Nodeh, R. Saidur, Novel magnetic graphene oxide functionalized cyanopropyl nanocomposite as an adsorbent for the removal of Pb (II) ions from aqueous media: equilibrium and kinetic studies, Environ. Sci. Pollut. Res., 25 (2018) 27122–27132.
[47] Y. Bian, Z. Bian, J. Zhang, A. Ding, S. Liu, L. Zheng, H. Wang, Adsorption of cadmium ions from aqueous solutions by activated carbon with oxygen-containing functional groups, Chin. J. Chem. Eng., 23 (2015) 1705–1711.
[48] L. Zhang, J. Wei, X. Zhao, F. Li, F. Jiang, M. Zhang, X. Cheng, Competitive adsorption of strontium and cobalt onto tin antimonate, Chem. Eng. J., 285 (2016) 679–689.
[49] V.C.G. Dos Santos, A. de P.A. Salvado, D.C. Dragunski, D.N.C. Peraro, C.R.T. Tarley, J. Caetano, Highly improved chromium (III) uptake capacity in modified sugarcane bagasse using different chemical treatments, Quim. Nova, 35 (2012) 1606–1611.
[50] S.J. Kleinübing, R.S. Vieira, M.M. Beppu, E. Guibal, M.G.C. da Silva, Characterization and evaluation of copper and nickel biosorption on acidic algae Sargassum filipendula, Mater. Res., 13 (2010) 541–550.
[51] S. Duan, R. Tang, Z. Xue, X. Zhang, Y. Zhao, W. Zhang, J. Zhang, B. Wang, S. Zeng, S. Dezhi, Effective removal of Pb (II) using magnetic Co0.6Fe2.4O4 micro-particles as the adsorbent: synthesis and study on the kinetic and thermodynamic behaviors for its adsorption, Colloids Surf. A Physicochem. Eng. Asp., 469 (2015) 211–223.
[52] T. Wen, F. Qu, N.B. Li, H.Q. Luo, A facile, sensitive, and rapid spectrophotometric method for copper (II) ion detection in aqueous media using polyethyleneimine, Arabian J. Chem., 10 (2017) S1680–S1685.
[53] T.R. Choudhury, T. Acher, M.N. Amin, S.B. Quraishi, A.I. Mustafa, Removal of arsenic (III) from groundwater by adsorption onto duckweed (Lemna minor), Int. Res. J. Pure Appl. Chem., 6 (2015) 120–127.
[54] S. Shrestha, G. Son, S.H. Lee, T.G. Lee, Isotherm and thermodynamic studies of Zn (II) adsorption on lignite and coconut shell-based activated carbon fiber, Chemosphere, 92 (2013) 1053–1061.

[55] H.R. Nodeh, H. Sereshti, Synthesis of magnetic graphene oxide doped with strontium titanium trioxide nanoparticles as a nanocomposite for the removal of antibiotics from aqueous media, RSC Adv., 6 (2016) 89953–89965.
[56] J. Febrianto, A.N. Kosasih, J. Sunarso, Y.H. Ju, N. Indraswati, S. Ismadji, Equilibrium and kinetic studies in adsorption of heavy metals using biosorbent: a summary of recent studies, J. Hazard. Mater., 162 (2009) 616–645.
[57] L. Lonappan, T. Rouissi, R.K. Das, S.K. Brar, A.A. Ramirez, M. Verma, R.Y. Surampalli, J.R. Valero, Adsorption of methylene blue on biochar microparticles derived from different waste materials, Waste Manage, 49 (2016) 537–544.
[58] K.M. Al-Qahtani, Water purification using different waste fruit cortexes for the removal of heavy metals, J. Taibah Univ. Sci., 10 (2016) 700–708.
[59] V. Doğan, S. Aydın, Vanadium (V) removal by adsorption onto activated carbon derived from starch industry waste sludge, Sep. Sci. Technol., 49 (2014) 1407–1415.
[60] A. Benhamou, M. Baudu, Z. Derriche, J.-P. Basly, Aqueous heavy metals removal on amine-functionalized Si-MCM-41 and Si-MCM-48, J. Hazard. Mater., 171 (2009) 1001–1008.
[61] F. Ciesielczyk, P. Bartczak, T. Jesionowski, Removal of cadmium (II) and lead (II) ions from model aqueous solutions using sol–gel-derived inorganic oxide adsorbent, Adsorption, 22 (2016) 445–458.